Stroncik, N.A., et al., 2017, Helium isotope evidence for a deep-seated mantle plume involved in South Atlantic breakup: Geology, doi:10.1130/G39151.1.

Sampling strategy, cosmogenic ^{3}He and in situ ^{4}He production

This study combines He and O isotopes of olivines with radiogenic isotope and trace element data from their respective host rocks. Samples were selected from a suite of olivine-phyric dolerite dykes in the Henties Bay - Outjo dyke swarm (HOD) in Namibia. These dykes have high Mg/(Mg+Fe) and high Cr and Ni contents, and contain fresh olivine. None of the samples represent primary mantle melts since they underwent differentiation and crustal contamination prior to or during emplacement. Crustal contamination can be a major issue for CFB in general, but for He isotopes in particular, since radiogenic ^{4}He from the decay of U and Th will lower primary ^{3}He/^{4}He signatures, and the country rocks to the HOD dykes are Neoproterozoic granitoids and pelitic metasediments with upper crustal U and Th contents (3 to 16 and 15 to 62 ppm, respectively; e.g. Jung et al., 1998). We used two different methods to tackle this problem: (1) we attempted to minimize contamination effects by selecting samples that appeared the least-differentiated and most accumulative; (2) we purposefully evaluated the degree of contamination using appropriate isotopic and trace element ratios (O, Sr, Nd, Pb, and Nb/U).

As all of the investigated samples are derived from surface outcrops, the primary ^{3}He/^{4}He may also be affected by cosmogenic ^{3}He due to exposure to cosmic ray irradiation. In order to minimize the effect of cosmogenic ^{3}He production, samples were taken from vertical rock faces (see Figure below) up to one meter below the top surface. This reduces the cosmogenic ^{3}He production by about a factor of two compared to a flat horizontal surface.

Typical dike outcrop resampled for this study. The block with the hammer on top is about 1 m in thickness. Samples typically were taken at the base of blocks such as this one.

To evaluate the significance of cosmogenic ^{3}He production for the investigated samples, we estimated the cosmogenic ^{3}He concentration in the sample suite based on typical erosion rates

prevailing in the area (Table 2 supplementary data). Note that the erosion rates used for this evaluation have been obtained from rocks of outcrops in close vicinity to those studied in this contribution (e.g. Bierman and Caffee, 2001). The cosmogenic ^{3}He concentration C in a steadily eroding surface of "infinite" age is given by $C = \Lambda P/(\rho \varepsilon)$, where Λ is cosmic-ray attenuation length (160 g/cm^2), P is production rate, ρ is density (3.0 g/cm^3) and ε is erosion rate (e.g. Niedermann, 2002). The ^{3}He production rates for the investigated surfaces (at 2π solid irradiation angle) vary from 115 to 180 atoms g^{-1} a^{-1}, depending on sample latitude and altitude (assuming a sea level, high latitude production rate of 124 atoms g^{-1} a^{-1}; Goehring et al., 2010; and scaling after Dunai, 2000), whereas typical bedrock erosion rates for the area are around 3.0 to 5.5 m Ma^{-1} (e.g. Bierman and Caffee, 2001). Using a conservative approach applying the lowest erosion rate, this results in cosmogenic ^{3}He concentrations ranging between 7.1×10^{-13} and 1.1×10^{-12} cm^3 STP g^{-1} in a sample from a flat horizontal surface, or at most 5.6×10^{-13} cm^3 STP g^{-1} in the vertical rock face samples that we used. Note that the lowest erosion rates have been obtained in quartzite samples (Bierman and Caffee, 2001). Studying cosmogenic He and Ne isotopes in the Karoo Basin, South Africa, Kounov et al. (2007) have shown that dolerites erode nearly twice as fast as quartzites, indicating that the effects of cosmogenic ^{3}He addition in the studied samples might be even lower than estimated using an erosion rate of 3m/Ma.

Given that samples are ~130 Ma in age, in-growth of ^{4}He from decay of ^{235}U, ^{238}U and ^{232}Th will also have a significant effect. The U and Th contents of the investigated olivines range between 6 and 100 ppb and between 51 and 350 ppb, respectively. Thus, between 29 and 290 $\times 10^{-8}$ cm^3 STP g^{-1} of ^{4}He have been produced by U and Th decay in the life-time of those samples. Consequently, a maximum ratio of cosmogenic ^{3}He to radiogenic ^{4}He of 1.4 R_A is obtained, implying that the production of cosmogenic ^{3}He is not only counter-balanced by the production of radiogenic ^{4}He (as both are produced within the crystal lattice or in melt inclusions) but that the measured $^{3}He/^{4}He$ ratios may even be considered as minimum values of the original composition. A negligible influence of cosmogenic He is also supported by the correlation of $^{3}He/^{4}He$ with other tracers of magma evolution (see main text).

Methods

Olivine separates for He isotope measurements were prepared by hand-picking of a 630-1000 µm sample fraction. To minimize the effects of radiogenic ^{4}He implanted from the rock matrix, the separates were leached in aqua regia (30 %) at room temperature for 30 minutes. In Table DR2 the percentage amount leached is listed. Note that samples KT-10-08 and KT-10-09 have not been leached. Those two samples show, in contrast to the others, extremly high ^{4}He concentrations in the 600°C step, indicating that the aqua regia treatment was successfully applied to eliminate the implanted radiogenic ^{4}He. Afterwards they were ultrasonically cleaned using acetone, wrapped in Al foil and placed into the sample carrousel of the extraction furnace or loaded into the crusher without wrapping. In order to discriminate the primary (magmatic) He signal from secondary (implanted and in situ produced) effects, gas extraction by heating was conducted in four temperature steps (600°C, 1000°C, 1400°C, 1750°C). We used a double-walled resistance furnace with a vacuum-tight Ta crucible fitted with a Mo liner. Mechanical extraction of gases was conducted in one step using a bellows-

tightened spindle press. Crusher blanks were run routinely before sample measurements and were between 2 and 10×10^{-12} cm^3 STP/g. Typical blank values for the extraction furnace were between 5 and 60×10^{-12} cm^3 STP, with the maximum value corresponding to the highest temperature steps. For details on the gas extraction and purification procedure see Niedermann et al. (1997). Noble gases were analyzed in a VG 5400 or Helix SFT mass spectrometer.

We chose stepwise heating as the main gas extraction method over the more common method of crushing for crystals obtained from the Earth's surface, because there are indications that crushing may also liberate gas components from the crystal lattice (e.g. Scarsi, 2000; Yokochi et al, 2005; Blard et al., 2006, 2008; Tolstikhin et al., 2010) and our laboratory experience shows that it is possible to resolve different He components in olivines by stepwise heating. The $^3He/^4He$ ratio of samples affected by cosmogenic He is highest in the lowest temperature step and then decreases with each step (Figs. 3s and 4s). In contrast, olivines derived from uncontaminated magmas not affected by in situ ^4He production or by cosmic irradiation yield constant $^3He/^4He$ ratios for all extraction steps (Figs. 3s and 4s). Olivines from continental settings often show complex release patterns with highly radiogenic (low) $^3He/^4He$ ratios in the lower temperature steps and variably higher $^3He/^4He$ ratios in the >600°C steps (e.g. Figs. 3s and 4s). Whereby the highest $^3He/^4He$ ratio not necessarily is always going to be released in the same temperature step, as this depends on the amount of radiohenic ^4He produced and the number of melt or fluid inclusions present in the olivine. The He release patterns of the samples studied here are relatively complex also (see Table DR1), reflecting the different origins of the He signal inherited by the olivine during its evolution. It has to be noted in this context that, with the exception of sample KT-10-11, the highest $^3He/^4He$ signal was not measured in the lowest temperature step. Sample KT-10-11 was taken as sort of a reference sample for assessing the differences in degassing patterns for samples of specific sample suite having been affected by cosmogenic ^3He production versus those who have not. Sample KT-10-11 was taken near the top of a dike on the top of a hill with virtually no shielding. As seen in Fig. 4s, it has a high $^3He/^4He$ ratio in the lowest temperature step, which drops very fast to ratios being even below the upper mantle ratio already in the next temperature step. This is in contrast to sample KT-10-03, which shows a constantly high $^3He/^4He$ signal in the 600, 1000 and 1400°C steps. Constantly high $^3He/^4He$ signals are only obtained from olivine having high mean forsterite content. In all other samples the primary He isotope signal is overprinted to variable degrees by wall rock assimilation and in situ produced ^4He. This is well illustrated by the positive correlation of the maximum $^3He/^4He$ with forsterite content for the two magmatic suites (Fig. 3). This implies that the maximum $^3He/^4He$ of each sample best reflects the most pristine magmatic value, but is a minimum estimate.

Oxygen isotopes were analyzed by laser fluorination at the University of Cape Town using methods described by Harris and Vogeli (2011). 1 to 3 mg of olivine was reacted with 10 kPa BrF_5. The O isotopes were measured on O_2 gas using a Finnigan Delta XP mass spectrometer in dual-inlet mode. Repeat analyses of internal garnet standard MON GT were used to normalize raw data and monitor precision. Data are reported in δ notation, where $\delta^{18}O = (R_{sample}/R_{standard} -1)*1000$, and R is the measured $^{18}O/^{16}O$ ratio. The $\delta^{18}O$ value of MON GT is 5.38 ‰, assuming 5.80 ‰ for the UWG-2 garnet standard of Valley et al. (1995). The long-

term average difference between MONGT standards in the same run is 0.11 per mil (n=216). This corresponds to a 1σ SD of 0.075 per mil.

Bulk-rock chemical analyses were made at the GFZ Potsdam using X-ray fluorescence and solution ICPMS techniques as described by Risse et al. (2013). Analyses of Sr, Nd and Pb isotopes followed standard acid digestion and cation exchange procedures described in detail by Romer et al. (2005). The isotopic compositions of Sr and Nd were analyzed on a Thermo-Fisher Triton mass spectrometer using dynamic multi-collection and normalized to $^{86}Sr/^{88}Sr$ = 0.1194 and $^{146}Nd/^{144}Nd$ = 0.7219, respectively. Lead was analyzed using static mean-collection of a Thermo-Fisher Triton mass spectrometer. Mass fractionation for Pb was corrected with a factor of 0.1 % per a.m.u., based on repeated measurements of reference material NBS981. During the measurement period, NBS987 Sr reference material and the LaJolla Nd reference material gave average $^{87}Sr/^{86}Sr$ and $^{143}Nd/^{144}Nd$ values of 0.710249±12 (2σ SD of 20 measurements) and 0.511850±7 (2σ SD of 11 measurements), respectively. Instrumental fractionation was corrected by 0.1% per a.m.u. as determined from the long-term reproducibility of Pb reference material NBS-981. The accuracy and precision of the reported Pb isotope ratios is better than 0.1% at the 2σ level of uncertainty.

References

Althaus T., Niedermann S. and Erzinger J. (2003): Noble gases in olivine phenocrysts from drill core samples of the Hawaii Scientific Drilling Project (HSDP) pilot and main holes (Mauna Loa and Mauna Kea, Hawaii). *Geochem. Geophys. Geosyst.* **4(1)**, 8701, doi:10.1029/2001GC000275.

Bierman, P. R. & Caffee, M. Slow rates of rock surface erosion and sediment production across the Namib desert and escarpment, southern Africa. *American Journal of Science* **301,** 326–358 (2001).

Blard, P.-H., Pik, R., Lavé, J., Bourlès, D., Burnard, P.G., Yokochi, R., Marty, B. & Trusdell, F. Cosmogenic ^{3}He production rates revisited from evidences of grain size dependent release of matrix-sited helium. *Earth and Planetary Science Letters* **247**, 222–234 (2006).

Blard, P.-H., Puchol, N. & Farley, K.A. Constraints on the loss of matrix-sited helium during vacuum crushing of mafic phenocrysts. *Geochimica et Cosmochimica Acta* **72**, 3788–3803, doi: 10.1016/j.gca.2008.05.044 (2008).

Blard P.-H., Balco G., Burnard P.G., Farley K.A., Fenton C.R., Friedrich R., Jull A.J.T., Niedermann S., Pik R., Schaefer J.M., Scott E.M., Shuster D.L., Stuart F.M., Stute M., Tibari B., Winckler G. and Zimmermann L. An inter-laboratory comparison of cosmogenic ^{3}He and radiogenic ^{4}He in the CRONUS-P pyroxene standard. *Quat. Geochron.* **26**, 11-19 (2015).

Dunai, T. J. Scaling factors for production rates of in situ produced cosmogenic nuclides: a critical reevaluation. *Earth and Planetary Science Letters* **176,** 147–156 (2000).

Fenton C.R., Niedermann S., Goethals M.M., Schneider B. and Wijbrans J. (2009): Evaluation of cosmogenic ^{3}He and ^{21}Ne production rates in olivine and pyroxene from two

Pleistocene basalt flows, western Grand Canyon, AZ, USA. *Quat. Geochron.* **4**, 475-492 (2009).

Fenton C.R. and Niedermann S. Surface exposure dating of young basalts (1-200 ka) in the San Francisco volcanic field (Arizona, USA) using cosmogenic ^{3}He and ^{21}Ne. *Quat. Geochron.* **19**, 87-105 (2014).

Goehring, B. M. *et al.* A reevaluation of in situ cosmogenic ^{3}He production rates. *Quaternary Geochronology* **5,** 410–418 (2010).

Harris, C. & Vogeli, J. Oxygen isotope composition of garnet in the peninsula granite, cape granite suite, South Africa: Constraints on melting and emplacement mechanisms. *South African Journal of Geology* **113,** 401–412 (2011).

Jung, S., Mezger, K. & Hoernes, S. Petrology and geochemistry of syn- to post-collisional metaluminous A-type granites—a major and trace element and Nd–Sr–Pb–O-isotope study from the Proterozoic Damara Belt, Namibia. *Lithos* **45**, 147-175 (1998).

Kounov, A., Niedermann, S., De Wit, M. J., Viola, G., Andreoli, M., & Erzinger, J. Present denudation rates at selected sections of the South African escarpment and the elevated continental interior basedon cosmogenic ^{3}He and ^{21}Ne. *South African Journal of Geology* **110**, 235-238 (2007).

Niedermann, S. Cosmic-Ray-Produced Noble Gases in Terrestrial Rocks: Dating Tools for Surface Processes. *Reviews in Mineralogy and Geochemistry* **47,** 731–784 (2002).

Niedermann, S., Bach, W. & Erzinger, J. Noble gas evidence for a lower mantle component in MORBs from the southern East Pacific Rise: Decoupling of helium and neon isotope systematics. *Geochimica et Cosmochimica Acta* **61,** 2697–2715 (1997).

Pilz P. Ein neues magmatisch-tektonisches Modell zur Asthenosphärendynamik im Bereich der zentralandinen Subduktionszone Südamerikas. Ph. D. Thesis, Universität Potsdam (2008).

Risse, A., Trumbull, R. B., Kay, S. M., Coira, B. & Romer, R. L. Multi-stage Evolution of Late Neogene Mantle-derived Magmas from the Central Andes Back-arc in the Southern Puna Plateau of Argentina. *Journal of Petrology* **54,** 1963–1995 (2013).

Romer, R. L. *et al.* Elemental dispersion and stable isotope fractionation during reactive fluid-flow and fluid immiscibility in the Bufa del Diente aureole, NE-Mexico: evidence from radiographies and Li, B, Sr, Nd, and Pb isotope systematics. *Contributions to Mineralogy and Petrology* **149,** 400–429 (2005).

Scarsi, P. Fractional extraction of helium by crushing of olivine and clinopyroxene phenocrysts: effects on the ^{3}He/^{4}He measured ratio. *Geochimica et Cosmochimica Acta* **64**, 3751–3762 (2000).

Schmitt A.K., Stockli D.F., Niedermann S., Lovera O.M. and Hausback B.P. Eruption ages of Las Tres Vírgenes volcano (Baja California): A tale of two helium isotopes. *Quat. Geochron.* **5**, 503-511 (2010).

Schimmelpfennig I., Williams A., Pik R., Burnard P., Niedermann S., Finkel R., Schneider B. and Benedetti L. Inter-comparison of cosmogenic in-situ ^{3}He, ^{21}Ne and ^{36}Cl at low latitude

along an altitude transect on the SE slope of Kilimanjaro volcano (3°S, Tanzania). *Quat. Geochron.* **6**, 425-436 (2011).

Tolstikhin, I., Kamensky, I., Tarakanov, S., Kramers, J., Pekala, M., Skiba, V., Gannibal, M. & Novikov, D. Noble gas isotope sites and mobility in mafic rocks and olivine. *Geochimica et Cosmochimica Acta* **74**, 1436–1447 (2010).

Valley, J. W., Kitchen, N., Kohn, M. J., Niendorf, C. R. & Spicuzza, M. J. UWG-2, a garnet standard for oxygen isotope ratios: Strategies for high precision and accuracy with laser heating. *Geochimica et Cosmochimica Acta* **59,** 5223–5231 (1995).

Yokochi, R., Marty, B., Pik, R. & Burnard, P. High $^{3}He/^{4}He$ ratios in peridotite xenoliths from SW Japan revisited: Evidence for cosmogenic ^{3}He released by vacuum crushing. *Geochemistry, Geophysics, Geosystems* **6**, doi: 10.1029/2004GC000836 (2005).

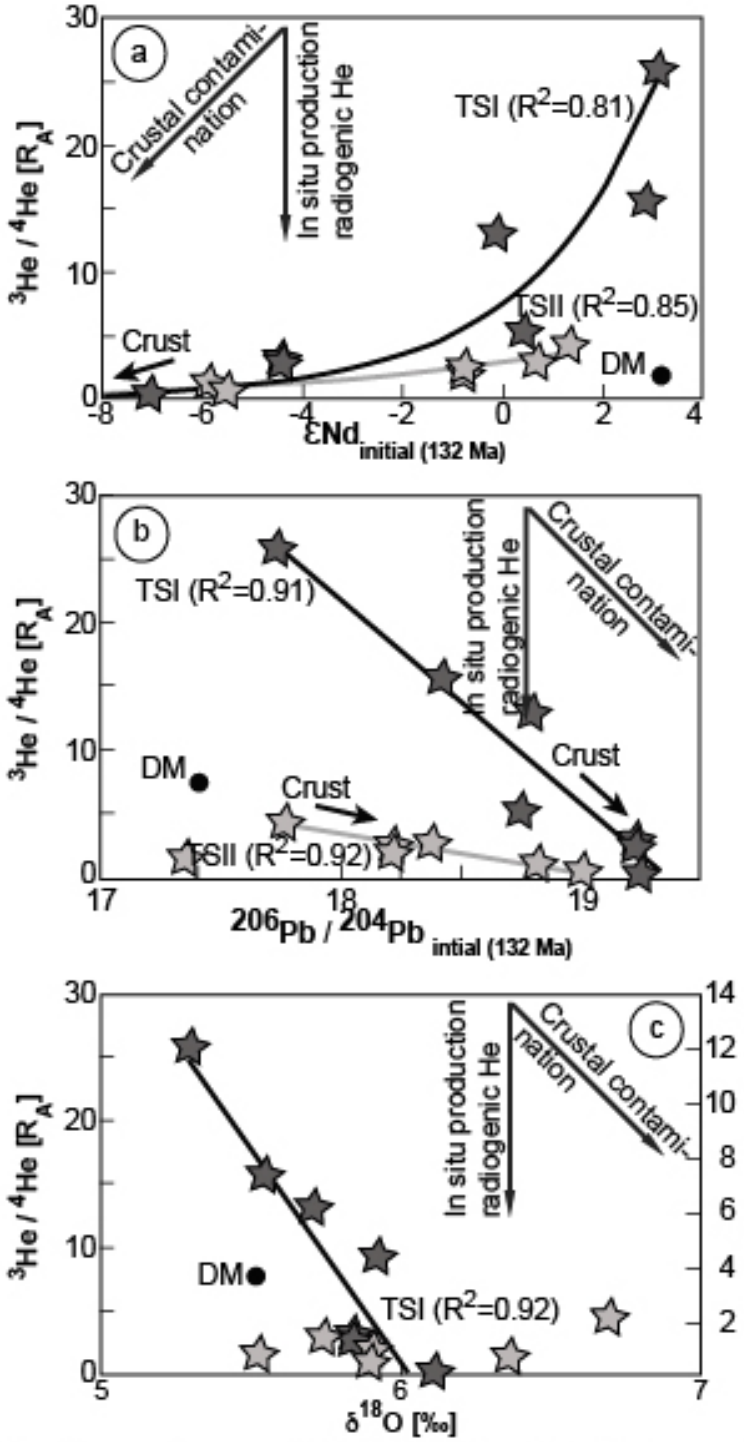

Figure 1s: He isotope ratios versus Nd (a), Pb (b), and O (c) isotope ratios. The black and the grey lines represent exponential and linear fits to the data of suites I and II, respectively. Note that fit I runs on one end through the sample with the most primitive 3He/4He ratio measured, whereas fit II runs through isotopic ratios typical for the depleted mantle (DM). Both fits run through isotopic ratios typical for the basement underlying the Etendeka flood basalts on the radiogenic end. The trends imply mixing between two different, isotopically distinct mantle sources.

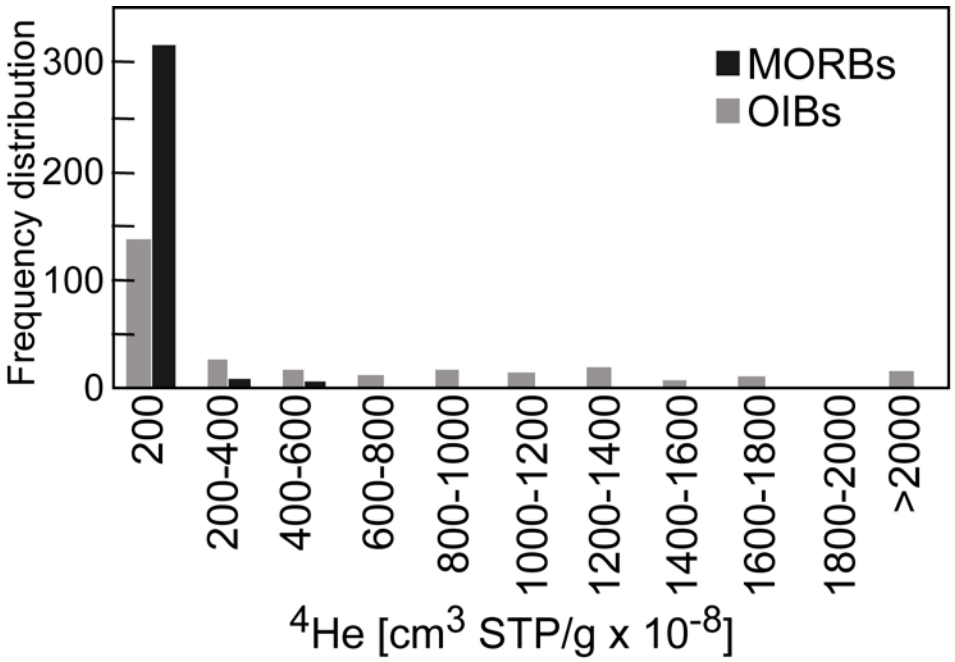

Figure 2s: Distribution of He concentration in MORBs and OIBs. Source of data is the same as in Graham (2002).

Graham, D. W. Noble gas isotope geochemistry of mid-ocean ridge and ocean island basalts: characterization of mantle source reservoirs. Reviews in Mineralogy and Geochemistry 47, 247–317 (2002).

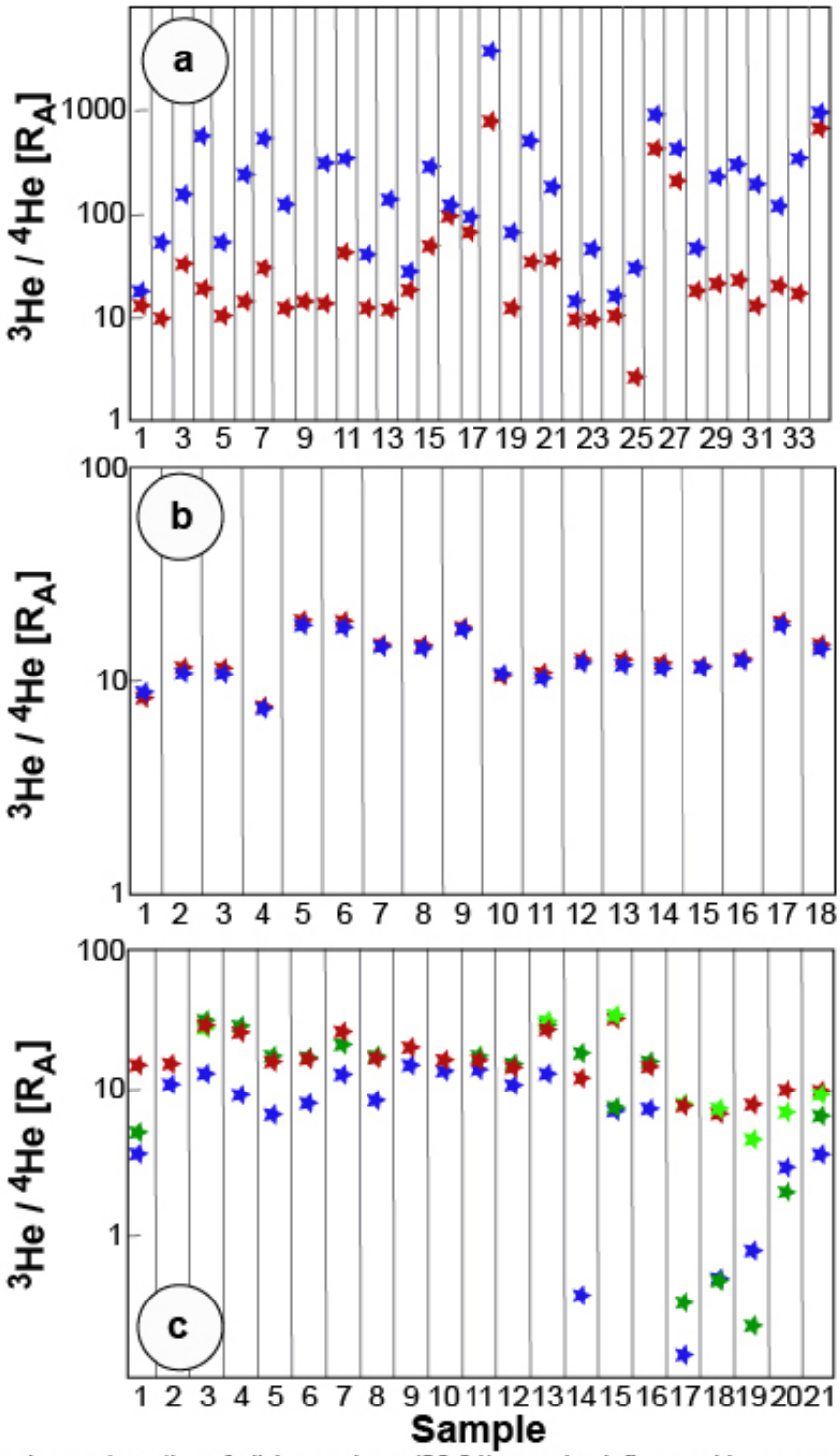

Fig. 3s: Degassing systematics of olivine and cpx (26-34) samples influenced by cosmogenic ^{3}He production (panel a), of fresh olivines derived from uncontaminated magmas (panel b), and of olivines derived from submarine emplaced lavas and from older magmas in continental settings showing signs of crustal contamination (panel c). Blue stars denote the lowest extraction temperature step, red stars the highest and green stars represent intermediate temperature extraction steps. Data source: Althaus et al. 2003; Blard et al., 2015; Fenton and Niedermann, 2014; Fenton et al., 2009; Mailer, 2009; Pilz, 2008; Schmitt et al., 2010; Schimmelpfennig et al., 2011

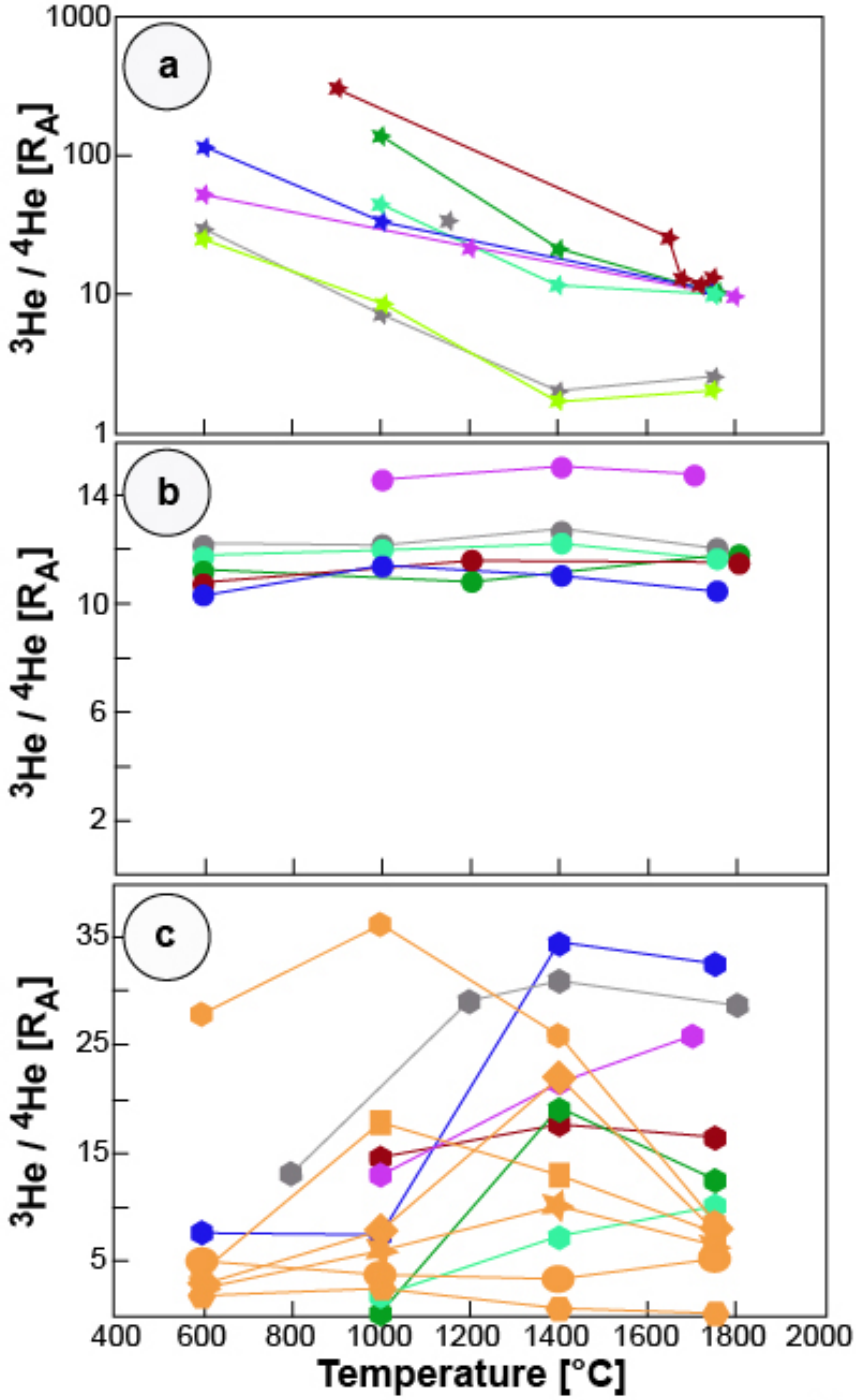

Fig. 4s: Characteristic degassing patterns of olivine samples influenced by cosmogenic ^{3}He production (panel a; not that the grey line and stars is sample KT-10-11 of this study), of fresh olivines derived from uncontaminated magmas (panel b), and from olivines derived from submarine emplaced, older lavas and from older lavas in continental settings showing signs of crustal contamination (panel c; note that orange samples are from this study). Different colors denote different samples. Data source same as in Figure 3s.

Sample ID	Temp	^{4}He	Error	^{3}He	Error	^{3}He/^{4}He	Error	^{3}He/^{4}He	Error	Fo range	Variance	Mg#	^{87}Sr/^{86}Sr	^{143}Nd/^{144}Nd	^{206}Pb/^{204}Pb	^{207}Pb/^{204}Pb	^{208}Pb/^{204}Pb	δ^{18}O	Nb	U
	[°C]	[10^{-8}]		[10^{-14}]		[10^{-6}]		R_A		olivine		whole rock								
KT-10-1 Top	**600**	6.40	0.32	46.5	3.4	7.27	0.39	5.23	0.28											
1.24616 g olivine	**1000**	42.5	2.1	205	12	4.83	0.17	3.47	0.12											
21°56.298 S	**1400**	50.7	2.5	171	10	3.379	0.090	2.431	0.065											
15°11.438 E	**1750**	0.0524	0.0028	0.42	0.17	8.1	3.2	5.8	2.3				0.708831	0.512567	19.67	15.72	38.96	5.84		
	Total	99.6	3.3	423	16	4.250	0.089	3.057	0.064	79-82	1	81	±0.000003	±0.000005					2.49	0.41
KT-10-1 Base	**600**	5.96	0.30	33.1	2.3	5.56	0.26	4.00	0.19											
1.21408 g olivine	**1000**	39.6	2.0	157.9	9.2	3.99	0.12	2.870	0.086											
21°56.298 S	**1400**	49.0	2.4	167	10	3.41	0.11	2.453	0.078											
15°11.438 E	**1750**	0.0398	0.0033	0.23	0.13	5.7	3.2	4.1	2.3				0.708831	0.512567	19.67	15.72	38.96	5.84		
	Total	94.6	3.2	358	14	3.79	0.08	2.725	0.056	79-82	1	81	±0.000003	±0.000005					2.49	0.41
KT-10-2	**600**	0.998	0.050	3.88	0.39	3.88	0.34	2.79	0.24											
1.0595 g olivine	**1000**	26.8	1.3	114.5	6.5	4.27	0.12	3.071	0.083											
21°16.729 S	**1400**	16.21	0.81	51.1	3.1	3.15	0.10	2.267	0.075											
14°20.418 E	**1750**	0.782	0.039	4.16	0.58	5.32	0.69	3.82	0.50				0.706852	0.512820	18.57	15.62	38.23	5.74		
	Total	44.8	1.6	173.6	7.2	3.87	0.08	2.787	0.059	75-85	8	79	±0.000003	±0.000005					3.50	0.15
KT-10-3 Base	**600**	0.339	0.017	9.57	0.97	28.2	2.5	20.3	1.8											
0.40712 g olivine	**1000**	2.98	0.15	107.1	6.2	35.9	1.0	25.85	0.74											
21°18.638 S	**1400**	4.19	0.21	109.5	6.5	26.14	0.83	18.80	0.60											
14°42.730 E	**1750**	1.036	0.052	9.25	0.89	8.93	0.74	6.43	0.53				0.707918	0.512875	17.88	15.59	37.68	5.30		
	Total	8.54	0.26	235.4	9.1	27.55	0.59	19.82	0.43	83-93	8	81	±0.000003	±0.000006					2.80	0.13
KT-10-5	**600**	3.10	0.16	9.4	1.2	3.03	0.37	2.18	0.27											
0.82816 g olivine	**1000**	6.53	0.33	118.4	7.4	18.13	0.68	13.04	0.49											
20°72.442 S	**1400**	1.98	0.10	26.0	2.0	13.11	0.79	9.43	0.57											
14°29.360 E	**1750**	0.253	0.013	2.20	0.57	8.7	2.2	6.3	1.6				0.706067	0.512774	19.08	15.67	38.59	5.71		
	Total	11.87	0.38	156.0	7.8	13.14	0.45	9.45	0.33	78-89	11	63	±0.000004	±0.000007					4.74	0.53
KT-10-7	**600**	0.233	0.012	0.74	0.17	3.17	0.72	2.28	0.52											
1.14142 g olivine	**1000**	1.549	0.077	12.50	0.92	8.07	0.43	5.81	0.31											
20°72.356 S	**1400**	0.656	0.033	14.3	1.7	21.8	2.4	15.6	1.7											
14°30.941 E	**1750**	0.251	0.013	2.06	0.46	8.2	1.8	5.9	1.3				0.704213	0.512928	18.73	15.61	38.22	5.55		
	Total	2.689	0.086	29.6	2.0	11.00	0.68	7.91	0.49	73-89	21	68	±0.000006	±0.000008					5.34	0.29
KT-10-7	**600**	0.445	0.018	1.23	0.17	2.77	0.36	1.99	0.26											
1.01156 g olivine	**1000**	1.795	0.072	14.32	0.64	7.98	0.16	5.74	0.11											
20°72.356 S	**1400**	0.772	0.031	10.28	0.56	13.32	0.50	9.58	0.36											
14°30.941 E	**1750**	0.1346	0.0055	0.884	0.086	6.57	0.58	4.72	0.42				0.704213	0.512928	18.73	15.61	38.22	5.55		
	Total	3.146	0.080	26.71	0.87	8.49	0.17	6.11	0.12	73-89	21	68	±0.000006	±0.000008					5.34	0.29
KT-10-8	**1000**	37.7	1.5	34.6	2.2	0.918	0.044	0.661	0.032											
0.11724 g olivine	**1400**	1.308	0.053	3.89	0.66	2.97	0.49	2.14	0.35											
20°46.031 S	**1750**	0.1664	0.0090	0.72	0.42	4.3	2.5	3.1	1.8				0.705013	0.512718	18.42	15.60	38.30			
14°34.696 E	**Total**	39.2	1.5	39.2	2.3	1.001	0.047	0.720	0.034	57-78	40	67	±0.000005	±0.000008					9.71	0.37

Table DR1

Sample ID	Temp	^{4}He	Error	^{3}He	Error	^{3}He/^{4}He	Error	^{3}He/^{4}He	Error	Fo range	Variance	Mg#	^{87}Sr/^{86}Sr	^{143}Nd/^{144}Nd	^{206}Pb/^{204}Pb	^{207}Pb/^{204}Pb	^{208}Pb/^{204}Pb	δ^{18}O	Nb	U
	[°C]	[10^{-8}]		[10^{-14}]		[10^{-6}]		R_A		olivine		whole rock								
KT-10-9	**1000**	101.8	4.1	59.1	4.7	0.580	0.040	0.417	0.029											
0.08064 olivine	**1400**	1.308	0.053	2.64	0.70	2.02	0.53	1.46	0.38											
20°48.516 S	**1750**	0.0526	0.0072	0.20	0.27	3.8	5.1	2.7	3.7				0.704888	0.512640	17.48	15.51	37.72			
14°33.784 E	**Total**	103.1	4.1	61.9	4.8	0.600	0.040	0.432	0.029	65-81	24	69	±0.000008	±0.000005					5.39	0.23
KT-10-10	**600**	0.0194	0.0011	0.031	0.046	1.6	2.4	1.2	1.7											
1.13526 g olivine	**1000**	70.0	3.5	172	10	2.463	0.070	1.772	0.051											
21°92.157 S	**1400**	240	17	96.9	8.3	0.404	0.019	0.291	0.014											
15°15.215 E	**1750**	0.938	0.047	0.38	0.10	0.41	0.11	0.293	0.076				0.708276	0.512521	19.34	15.70	38.89	5.90		
	Total	311	17	270	13	0.868	0.038	0.625	0.027	74-78	1	77	±0.000005	±0.000008					3.13	0.38
KT-10-11	**600**	4.98	0.25	145.7	8.1	29.27	0.69	21.06	0.50											
1.13418 g olivine	**1000**	40.9	2.0	300	17	7.32	0.21	5.26	0.15											
21°92.660 S	**1400**	69.4	3.5	139.5	8.0	2.009	0.058	1.445	0.041											
15°16.228 E	**1750**	0.0201	0.0012	0.053	0.054	2.6	2.7	1.9	1.9				0.707135	0.512508	19.00	15.71	38.89	6.11		
	Total	115.4	4.0	585	21	5.07	0.14	3.65	0.10	73-81	7	74	±0.000007	±0.000008					4.82	0.32
412	**600**	8.96	0.45	21.5	3.2	2.40	0.34	1.72	0.24											
0.45654 g olivine	**1000**	1.415	0.071	4.00	0.58	2.82	0.38	2.03	0.27											
	1400	28.3	1.4	163	10	5.75	0.17	4.14	0.12											
	1750	1.386	0.069	14.6	1.5	10.56	0.97	7.60	0.70				0.704392	0.512836	17.98	15.52	37.74	6.70		
	Total	40.1	1.5	203	10	5.07	0.14	3.64	0.10	72-84	12	65	±0.000007	±0.000009					8.10	0.28
Q22	**crushe**	96.5	4.8	166	14	1.73	0.12	1.241	0.088	73-83	14	77	0.707705	0.512482	19.03	15.70	39.03	6.36	4.30	0.27
0.17766 g olivine													±0.000007	±0.000008						
KT-10-8	**crushe**	0.705	0.036	2.46	0.75	3.5	1.0	2.51	0.75	57-78	40	67	0.705013	0.512718	18.42	15.60	38.30		9.71	0.37
0.15896 g olivine													±0.000005	±0.000008						
JDNM05	**crushe**	0.280	0.014	2.09	0.39	7.5	1.4	5.36	0.97										14.30	0.73
0.77708 g olivine																				
JDNM09	**crushe**	0.916	0.046	9.7	1.0	10.6	1.0	7.65	0.73										3.60	0.34
1.0013 g olivine																				

Note that the indicated errors are 2Sigma errors.